Potential of microwave observations for the evaluation of rainfall and convection in a regional climate model in the frame of HyMeX and MED-CORDEX

Jean-François Rysman, Ségolène Berthou, Chantal Claud, Philippe Drobinski, Jean-Pierre Chaboureau, Julien Delanoë

Potential of microwave observations for the evaluation of rainfall and convection in a regional climate model in the frame of HyMeX and MED-CORDEX

Jean-François Rysman · Ségolène Berthou · Chantal Claud · Philippe Drobinski · Jean-Pierre Chaboureau · Julien Delanoë

Abstract This study evaluates the potential of spaceborne passive microwave observations for assessing decadal simulations of precipitation from a regional climate model through a model-to-satellite approach. A simulation from the Weather and Research Forecasting (WRF) model is evaluated against 2002-2012 observations from the Advanced Microwave Sounding Unit (AMSU-B) and the Microwave Humidity Sounder (MHS) over the Mediterranean region using the radiative transfer code RTTOV (Radiative Transfer for Tiros Operational Vertical Sounder). It is first shown that simulated and observed brightness temperatures are consistently correlated for both water vapour and window channels. Yet, although the average simulated and observed brightness temperatures are similar, the range of brightness temperatures is larger in the observations. The difference is presumably due to the too low content of frozen particles in the simulation. To assess this hypothesis, density and altitude of simulated frozen hydrometeors are compared with observations from an airborne cloud radar. Results show that simulated frozen hydrometeors are found at lower median altitude than observed frozen hydrometeors, with an average content at least 5 times inferior. Spatial distributions of observed and simulated precipitation match reasonably well. However, when using simulated brightness temperatures to diagnose rainfall, the simulation performs very poorly. These results highlight the need of providing more realistic frozen hydrometeors content, which will increase the interest of using passive microwave observations for the long-term evaluation of regional models. In particular, significant improvements are expected from the archiving of convective fluxes of precipitating hydrometeors in future regional model simulation programs.

Keywords Convection · HyMeX · MED-CORDEX · Passive microwave observations · Precipitation · Radar observations · Radiative transfer model · Regional model

JF Rysman
Laboratoire de Métérology Dynamique Institut Pierre Simon Laplace
CNRS
École Polytechnique
Université Paris-Saclay
91120 Palaiseau, France
E-mail: jfrysman@lmd.polytechnique.fr

S. Berthou
LMD/IPSL, CNRS and École Polytechnique, Université Paris-Saclay, Palaiseau, France
C. Claud
LMD/IPSL, CNRS and École Polytechnique, Université Paris-Saclay, Palaiseau, France
P. Drobinski
LMD/IPSL, CNRS and École Polytechnique, Université Paris-Saclay, Palaiseau, France
JP Chaboureau
Laboratoire d'Aérologie, Université de Toulouse, CNRS, UPS, France
J. Delanoë
Laboratoire Atmosphères Milieux Observations Spatiales, IPSL, UVSQ, CNRS, UPMC

1 Introduction

Water shortage and floods are some of the main climatic challenges faced by the Mediterranean countries critically impacting their socio-economic vitality, threatening lives, causing damages to property, affecting the energy and transportation sectors (Drobinski et al, 2014). There are gaps in our understanding of the processes controlling the

Mediterranean precipitation which limit our ability to simulate properly its variability and trend in a warming climate (e.g., Barkhordarian et al, 2013). Such limitations are partially caused by the contribution of fine-scale processes (Rysman et al, 2016) and their non-linear interactions with large-scale processes as well as the complex and not well known interactions between oceanic, atmospheric and hydrological processes (e.g., Funatsu et al, 2009; Berthou et al, 2015). Large-scale atmospheric circulation together with the Mediterranean Sea act as a moisture and heat source for precipitation over the region (Duffourg and Ducrocq, 2011, 2013; Sodemann and Zubler, 2010; Pastor et al, 2015) while the mountains surrounding the Mediterranean Sea play a crucial role in rising air flow, which can lead to high-impact weather systems such as heavy precipitation. Cyclones, interactions with topography and self-organisation of convection are typical mechanisms that can localize precipitation systems fed by low-level moist jets and induce very high precipitation amounts (Jansà et al, 2001; García-Herrera et al, 2005; Houze, 2004; Ducrocq et al, 2008; Argence et al, 2008; Pastor et al, 2010; Bresson et al, 2012; Ricard et al, 2012). The numerous rivers originating from the mountains can lead to flash floods with dramatic consequences in the very urbanised littorals of the Mediterranean (886 casualties in Algiers in November 2001, 20 casualties in Draguignan in June 2010). A better understanding of the processes associated with precipitation is also of importance regarding their direct impact on aquifer recharge, river discharge, soil water content and vegetation characteristics specific to the Mediterranean basin.

The Hydrological cycle in the Mediterranean eXperiment (HyMeX, Drobinski et al (2014)) is a 10-year concerted experimental effort at the international level aiming at advancing the scientific knowledge of the water cycle variability in all compartments (land, sea and atmosphere) and at various temporal and spatial scales. It also aims at improving the regional climate models ability for predicting regional climate variability and evolution in coordination with the MED-CORDEX program (Ruti et al, 2015). A wealth of observations (Ducrocq et al, 2014) and simulations (Ruti et al, 2015) have been collected in the HyMeX database since 2010 such as observations from passive microwave sounders on-board satellites and simulations performed in the context of the joint HyMeX/MED-CORDEX initiative. This database is thus particularly worthwhile to study precipitation combining different methods and approaches.

The regional climate simulations cover the ERA-Interim period 1989-2008 as initially recommended in the MED-CORDEX project. Some simulations were extended afterwards to cover the updated ERA-Interim period 1979-2008 and the HyMeX observation periods from September 2012 to April 2013. Several regional climate models (RCM) have been run in atmosphere-only mode where the ERA-Interim sea-surface temperature (SST) was prescribed as the lower boundary conditions, while some other simulations used atmosphere-ocean regional climate models (AORCM) with SST prognosed at each time step by the ocean model as a lower boundary condition to the RCM. All models provide the meteorological variables controlling precipitation triggering with a 3-h temporal resolution and an horizontal 20 km grid-spacing over a large domain encompassing the Mediterranean Sea, parts of Europe and North Africa (14.3 $^\circ$ W - 42.3 $^\circ$ E/ 28.3 $^\circ$ N - 51.3 $^\circ$ N).

Passive microwave sounders are powerful tools to monitor the atmosphere over land and sea. They have been primarily developed to measure temperature and humidity profiles (Susskind et al, 1984; Gloersen and Barath, 1977) and to retrieve total precipitable water (Wang et al, 1989), but many other atmospheric applications have been developed since then; such as hail and convection detection (Ferraro et al, 2015; Hong et al, 2005a) and rain rate retrieval (Laviola and Levizzani, 2011; Kidd et al, 2016). These instruments probe the atmosphere at frequencies from 20 to 200 GHz using several channels often centered in the oxygen bands (for temperature profiling) and water vapour bands (for humidity profiling). Since the first generation of instruments launched in the seventies (e.g., Scanning Microwave Spectrometer (SCAMS) (Staelin et al, 1975), Microwave Sounding Unit (MSU)), much improvement has been brought in terms of sensitivity, accuracy and resolution. At present the lastest generation offers 10-20 km resolutions at nadir with a swath width of 2000 km. Among them, the Advanced Microwave Sounding Unit (AMSU-B) (Vangasse et al, 1996) and the Microwave Humidity Sounder (MHS) (Bonsignori, 2007) are two very similar instruments that probe the atmosphere using two window channels and three water vapour channels with a 16 km resolution at nadir. Since 1999, they have been installed on-board seven polar orbiting satellites and, since 2002, at least 3 instruments have been operational

together. This ensures a fair temporal resolution in the Mediterranean (of about 3 to 4 hours). Moreover, in the coming years, similar radiometers will be launched (e.g., MHS on Metop-C, 2018, and Advanced Technology Microwave Sounder (ATMS) on Joint Polar Satellite System 1-4 (JPSS 1-4), 2017, 2021, 2026, 2031) that will extend the already considerable span of this database. Note that a first ATMS has been launched on board the Suomi National Polar-orbiting Partnership (Suomi NPP) satellite in October 28, 2011, and is fully operational since March 2012.

Such a long-term and homogeneous database can be worthwhile for the evaluation of regional climate models over decadal periods and for the understanding of precipitation variability at various temporal and spatial scales. Moreover, the spatial and temporal resolutions of the database are very similar to those of the MED-CORDEX simulations allowing a straightforward comparison. A preliminary attempt to evaluate a regional climate model using these passive microwave sounders has been performed by Claud et al (2012). The simulated rain rate was compared to the diagnosed rain occurrence from AMSU-B, with a fair qualitative agreement. This study goes one step further in the evaluation of regional climate model simulations by simulating the brightness temperatures of model outputs with the Radiative Transfer for Tiros Operational Vertical Sounder (RTTOV-v11) (Saunders et al, 2013). The simulation of brightness temperatures allows the direct comparison with satellite observations. With this method, the satellite observations do not need any retrieval procedures and their associated unknown errors. The sole uncertainties associated with the measurements are limited to the known issues on sensor calibration. In the past, the so-called model-to-satellite approach was extensively used for microwave instruments on cloud-resolving model outputs for building microphysics database (e.g., Panegrossi et al, 1998; Marzano et al, 1999; Kummerow et al, 2001; Michele et al, 2005; Meirold-Mautner et al, 2007; Chaboureau et al, 2008; Defer et al, 2008; Casella et al, 2013; Sanò et al, 2013) or assessing simulations (e.g., Wiedner et al, 2004; Surussavadee and Staelin, 2006; Clark and Chaboureau, 2010) covering short periods of time (typically a few days).

The objective of this study is to assess the potential of microwave observations to evaluate decadal simulations of a regional climate model using a model-to-satellite approach. A special attention is dedicated to the evaluation of precipitation and associated microphysics.

The dataset and the methodology are detailed in section 2. Section 3 is dedicated to the assessment of simulated brightness temperatures. Then, in section 4, we assess the simulated frozen hydrometeors against observations collected during the HyMeX first Special Observation Period (SOP-1) and we study the sensitivity of simulated brightness temperatures to the frozen hydrometeors shape in section 5. Finally, in section 6, we evaluate the simulated rainfall occurrence against the observed rainfall occurrence. These results are discussed in the last section of the paper.

2 Data and Methods

2.1 The Advanced Microwave Sounding Unit (AMSU-B) and the Microwave Humidity Sounder (MHS)

This study uses brightness temperature measurements from two passive microwave sounders: AMSU-B and MHS. These two very similar instruments measure upwelling microwave radiation with nearly identical frequencies: two window channels at 89 and 150 GHz (AMSU-B)/157 GHz (MHS) and three channels in the water vapour absorption line at 183.3±1, 183.3±3, and 183.3±7 (AMSU-B)/190.3 GHz (MHS). Their swath width is approximately of 2000 km, their nadir resolution is 16 km and their viewing angles go up to about 60°. The first AMSU-B was launched in 1998 on the National Oceanic and Atmospheric Administration 15 (NOAA-15) polar orbiting satellite. Since then, six more instruments were launched in 2001 (AMSU-B/NOAA-16), 2002 (AMSU-B/NOAA-17), 2005 (MHS/ NOAA-18), 2007 (MHS/Meteorological Operational satellite A (MetOp-A)), 2009 (MHS/NOAA-19), and 2012 (MHS/MetOp-B). In this study, we used measurements from 2002 to 2012 in order to ensure that at least 3 instruments are available simultaneously, which allows a temporal resolution of about 4 h. The measured brightness temperature field was re-interpolated on the model grid (bi-linear interpolation).

Several authors studied the effect of surface emissivity, water vapour and hydrometeors on simulated brightness temperature in the microwaves (e.g., Mugnai and Smith, 1988; Mugnai et al, 1990; Smith et al, 1992; Kummerow and Giglio, 1994; Petty, 1995; Panegrossi et al, 1998; Stephens and Kummerow, 2007), and more specifically for AMSU-B and MHS channels (e.g., Burns et al, 1997; Fer-

raro et al, 2000; Bennartz and Petty, 2001; Skofronick-Jackson et al, 2002; Bennartz and Bauer, 2003; Hong et al, 2005b; Surussavadee and Staelin, 2006; Laviola and Levizzani, 2011). They highlighted some systematic characteristics that are listed in the following. First, the channels of a microwave radiometer probe more or less deep in the atmosphere depending on their frequencies. Under clear sky conditions, AMSU-B and MHS weighting functions peak at the ground level for window channels and mainly from 2 km (183.3±7 GHz) to 8 km (183.3±1 GHz) for water vapour channels (e.g., Karbou et al (2005) for mid-latitudes). Therefore, each channel of AMSU-B/MHS is sensitive to a different layer of the atmosphere. For example, the water vapour channels are nearly insensitive to low-levels clouds. Second, the radiation measured by the microwave radiometers depends on: the emission of the surface and/or the atmosphere and the emission, absorption and scattering by atmospheric components (water vapour, cloud liquid water, rain and frozen hydrometeors). Thus, the measured brightness temperatures of AMSU-B and MHS depend on the channel frequency, on the surface properties, on the vertical profiles of water vapour and temperature and on the density, phase, shape, size distribution and altitude of hydrometeors.

In greater details, the 89 GHz channel is sensitive to rain, surface emissivity, water vapour, cloud liquid water and frozen hydrometeors while the 150/157 GHz channel is slightly sensitive to surface emissivity, insensitive to rain and strongly sensitive to cloud liquid water, water vapour and frozen hydrometeors (Bennartz and Bauer, 2003; Deeter and Vivekanandan, 2005; Hong et al, 2005b; Surussavadee and Staelin, 2006). Both window channels are globally insensitive to atmosphere temperature. The water vapour channels are sensitive to the atmosphere temperature, the water vapour and the hydrometeors. In particular, they are very sensitive to high density frozen hydrometeors (such as graupel and hail). Moreover, they are nearly insensitive to surface properties (i.e., temperature and emissivity, except for very dry and cold atmosphere (see Laviola and Levizzani (2011))). Because the 183.3±7 channel probes deeper in the atmosphere, it is also moderately sensitive to rain and cloud liquid water (Bennartz and Bauer, 2003). A comprehensive description of the impact of hydrometeors on the 89-183 GHz channels can be found in Laviola and Levizzani (2011).

Figure 1 shows an insightful example of brightness temperature measured by a MHS radiometer for a window channel (89 GHz) and a water vapour channel (190.3 GHz) on 12 October 2012 at 13:12 UTC. The 89 GHz channel is strongly affected by surface emissivity with a sharp contrast of brightness temperature between land and sea. In addition, the brightness temperature shows a strong variability over the sea with brightness temperature mainly ranging between 210 and 245 K. This variability is due to the presence of hydrometeors (precipitating and non-precipitating) and water vapour in the region. The low brightness temperatures over the Gulf of Lion are associated with clear-sky conditions while elsewhere images from the SEVIRI imager on-board the Meteosat Second Generation satellite reveal the presence of low-level clouds (not shown). Furthermore, a region of very low brightness temperatures (down to 180 K) is observed on the southern part of Majorca.

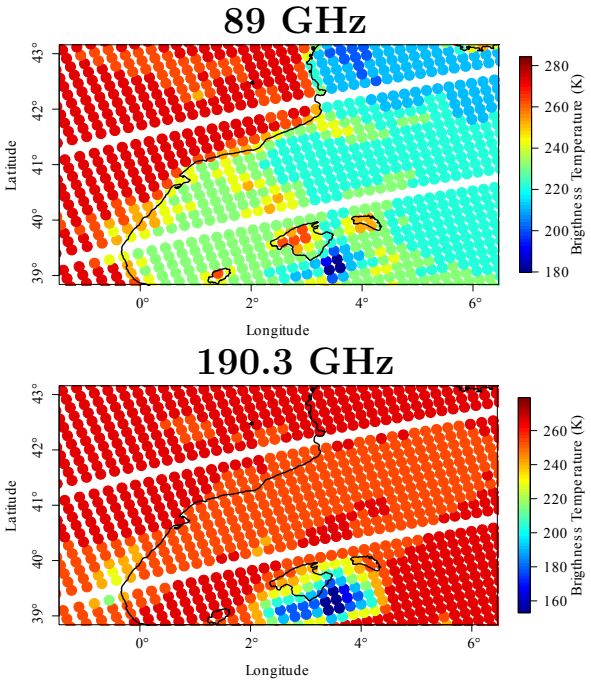

Fig. 1 Brightness temperature from MHS (NOAA-18) for channel 89 GHz (top) and channel 190.3 GHz (bottom) on a case study from the 12 October 2012 at 13:12 UTC.

The 190.3 GHz channel brightness temperatures range mainly from 230 to 270 K without any obvious influence of the surface properties. A very strong temperature depression is noticeable on the southern part of Majorca with brightness temperatures 100 K lower than in the surrounding regions. A significant temperature depression is also noticeable for 183.3±1 GHz channel in the same region (not shown here but see Figure 6), highlighting a

strong frozen hydrometeors loading in this convective region. This example illustrates the potential of the microwave radiometers to document some characteristics of the atmosphere and to provide insights about the vertical structure of liquid or solid atmospheric water.

2.2 Detection of rainfall and deep convection using AMSU-B/MHS

Several authors (Weng et al, 2003; Ferraro et al, 2005; Surussavadee and Staelin, 2008a,b; Laviola and Levizzani, 2011; Sanò et al, 2015) developed algorithms to detect and/or estimate precipitation using AMSU/MHS radiometers based on the properties described in the previous section. In this study, we use the algorithm developed by Funatsu et al (2007) which is particularly attractive from its simplicity and because it has been developed and calibrated in the Mediterranean region. The algorithm detects rainfall when the following criterion is fulfilled:

$$TB_3 - TB_5 \geq T_0 \tag{1}$$

where $TB_{3,5}$ are brightness temperatures for channels 3, 5 (i.e., 183.3±1 GHz, and 183.3±7 GHz for AMSU-B, and 183.3±1 GHz and 190.3 GHz for MHS) and T_0=-8 K. Rain from low-level clouds can be missed using this diagnostic. Funatsu et al (2007) showed the T_0 value corresponds to a rain rate most of the time greater than 10 mm/3 h.

In this study, we also use a diagnostic developed by Hong et al (2005a) to detect deep convection occurrence. Deep convection is detected whenever:

$$\begin{aligned} & TB_3 - TB_5 \geq T_0 \\ \textit{and} \quad & TB_3 - TB_4 \geq T_0 \\ \textit{and} \quad & TB_4 - TB_5 \geq T_0 \end{aligned} \tag{2}$$

with $T_0 = 0.04761 - 0.01678\ \theta + 0.00599\ \theta^2$ where θ is the viewing angle. This diagnostic has been primarily developed for tropical regions yet it has been validated thereafter in the Mediterranean region by Funatsu et al (2007); Rysman et al (2015).

2.3 The RAdar SysTem Airborne (RASTA)

In this study, we also use measurements from an airborne 95 GHz Doppler cloud radar named RASTA (Protat et al, 2004; Bouniol et al, 2008; Protat et al, 2009; Delanoë et al, 2013). During the HyMeX SOP-1, RASTA was installed on-board an aircraft which carried out 18 flights (about 50 flight hours) (Ducrocq et al, 2014). This instrument measures reflectivity using six antennas: three pointing downwards in three non-collinear directions, including one nadir pointing angle, and three pointing upwards in three non-collinear directions, including one zenith pointing angle. It has vertical and temporal resolutions of 60 m and 1.25 seconds, respectively. The calibration accuracy is about 1-2 dB and the lowest cloud reflectivity measurable is about -35 dBZ depending on the antenna. This instrument is used to investigate microphysical properties of clouds (e.g., Delanoë et al, 2013); mean volume-weighted diameter of frozen hydrometeors and ice water content being retrieved at each radar gate (i.e., 60 m) using the radonvar method (adapted from Delanoë et al, 2007, 2014). Hydrometeors with diameters ranging from approximately a hundred micrometers to a few millimetres are detected. A first evaluation using collocated in-situ measurements such as particle size and bulk measurements highlighted a retrieval error within 30 % for ice water content.

2.4 The Weather Research and Forecasting Regional Climate Model (WRF-RCM)

The model used in this study is the version 3.1.1 of the Weather Research and Forecasting Model (WRF). WRF is a limited area model, non-hydrostatic, with terrain following eta-coordinate mesoscale modeling system designed to serve both operational forecasting and atmospheric research needs (Skamarock et al, 2008). The WRF simulation has been performed in the context of the MED-CORDEX program, using a 20-km horizontal resolution grid that extends from 14.3 °W to 42.3 °E and from 28.3 °N to 51.3 °N between 1989 and 2014. Its initial and boundary conditions are provided by the ERA-Interim reanalysis of the European Centre for Mean-range Weather Forecasts (ECMWF) and updated every 6 hr (Simmons et al, 2007; Dee et al, 2011). In the vertical, 28 unevenly spaced levels are used and the atmosphere top is at 50 hPa. Topography data originate from 5-min resolution United States Geophysical Survey data. Soil type is based on a combination of the 10-min 17-category United Nations Food and Agriculture Organization soil data and U.S. State Soil Geographic 10-min soil data. A complete set of parameterizations is used. These include the WRF Single-Moment 5-class microphysical parameterization (Hong et al, 2004),

the new Kain-Fritsch convective parameterization (Kain, 2004), the Dudhia shortwave radiation (Dudhia, 1989) and Rapid Radiative Transfer Model longwave radiation (Mlawer et al, 1997), the Yonsei University planetary boundary layer scheme (Noh et al, 2003) and the Rapid Update Cycle (RUC) land-surface models (Smirnova et al, 1997, 2000). The WRF simulation has been relaxed towards the ERA-Interim large scale fields with a nudging time of 6 hr (Salameh et al, 2010; Omrani et al, 2013, 2015). With this set of parameterizations, water can be exchanged between water vapour, cloud water (liquid water within a cloud), rain (precipitating liquid water with a particle density of 1000 kg/m^3), ice (frozen water within a cloud) and snow (precipitating frozen water with a particle density of 100 kg/m^3). This allows for mixed-phase processes, super-cooled water and snow melt in addition to ice sedimentation.

The simulation provides the 3-hourly convective (i.e., subgrid) and non-convective precipitation field. The precipitation field has been evaluated over land against ECA&D (European Climate Assessment and Data set (Haylock et al, 2008)) and SAFRAN (Système d'analyse fournissant des renseignements atmosphériques à la neige (Quintana-Seguí et al, 2008)) raingauge-based gridded products at the Mediterranean basin scale (Stéfanon et al, 2014; Lebeaupin-Brossier et al, 2013; Flaounas et al, 2013; Berthou et al, 2014, 2015) and over sea against the satellite product of the Hamburg Ocean Atmosphere Parameters and fluxes from Satellite data (HOAPS) available twice a day with a spatial resolution of 0.5 $^\circ$ in longitude and latitude (Lebeaupin-Brossier et al, 2015). AMSU-B/MHS sounders appear as a complementary approach to evaluate the simulation at finer temporal (3-4 h) and spatial (16 km at nadir) resolutions with an homogeneous precipitation information over land and sea. The cloud coverage has also been evaluated in (Chakroun et al, 2016).

Two twin simulations with these specifications have been run with atmosphere-only mode and with atmosphere-ocean coupled mode (see Drobinski et al, 2012; Lebeaupin-Brossier et al, 2015). In this paper, we only present the results for runs in atmosphere-only mode because the results are very similar to those of the atmosphere-ocean coupled mode. The reasons for this similarity are discussed in the last section of this article.

2.5 RTTOV

The brightness temperatures of model outputs were computed using the radiative transfer model RTTOV (Radiative Transfer for Tiros Operational Vertical Sounder) version 11 (Saunders et al, 2013). This radiative transfer model was developed initially at ECMWF (Eyre, 1991; Saunders et al, 1999; Matricardi et al, 2004; Saunders et al, 2005) then within EUMETSAT NWP Satellite Application Facility. RTTOV is well designed to simulate brightness temperatures for the very large number of profiles of WRF simulations as it is able to compute very quickly a large number of satellite radiances from model outputs. The TELSEM (a Tool to Estimate Land Surface Emissivities at Microwave frequencies) atlas (Aires et al, 2011) was used to provide the surface emissivity of land while the FASTEM code was used for the surface emissivity of sea. Until recently, RTTOV simulated hydrometeors as spherical particles of different densities (e.g., 1000 kg/m^3 for rain, 100 kg/m^3 for snow). Yet, several studies (Kim et al, 2007; Geer and Baordo, 2014; Guerbette et al, 2016) showed that, when using this assumption, RTTOV had difficulties to provide realistic scattering from frozen hydrometeors simultaneously at every microwave frequency. Therefore, a new approach taking frozen hydrometeors as three-dimensional realistic shapes (e.g., Short Column, 3-Bullet Rosette, and Sector Snowflake) has been implemented. Geer and Baordo (2014) identified the "Sector Snowflake" shape, from those available in the Liu (2008) database, as the one that produces the best fit between global observations and ECMWF simulations for frequencies ranging from 10 to 183 GHz. This shape is used, as a first step, in sections 3 and 4 then a sensitivity test is conducted in section 5 to identify the most appropriate shape regarding the specific conditions of this study. The standard particle size distributions have been used, i.e., Marshall-Palmer for rain, mid-latitude Field et al (2007) for snow and modified-gamma for cloud-water and cloud-ice.

3 Evaluation of simulated brightness temperatures

Taylor diagrams (Taylor, 2001) provide a concise statistical summary of the performance of a model (Fig. 2). Specifically, Taylor diagrams highlight four different statistical properties of a given physical variable on a bi-dimensional polar diagram: the

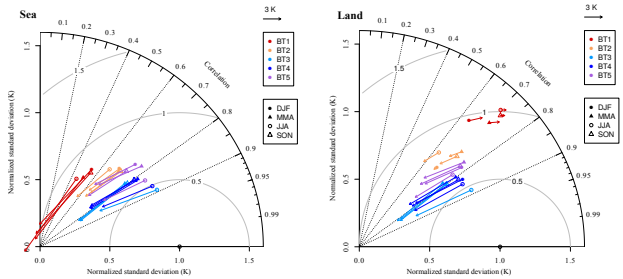

Fig. 2 Normalised Taylor diagrams comparing brightness temperatures (BT) of microwave sounder channels with their equivalent simulations from WRF for sea and land per channels and per seasons. Arrows indicate the magnitude and sign of the bias: an arrow directed to the left (right) indicates a negative (positive) bias.

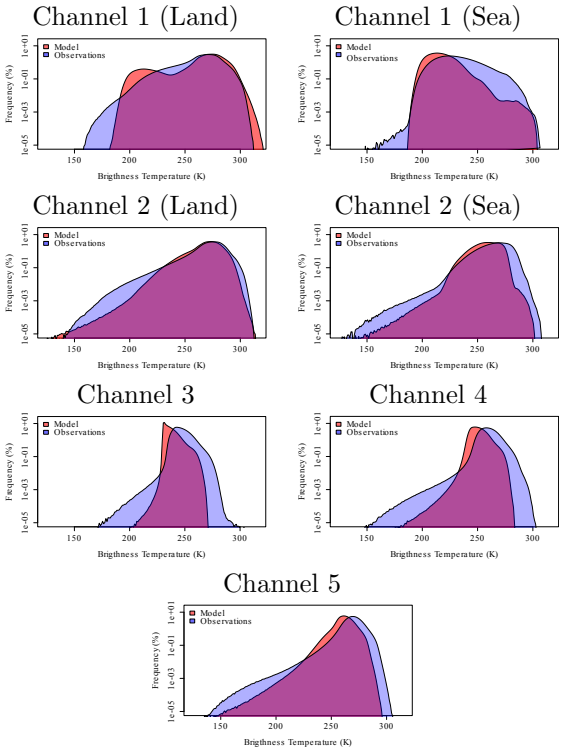

Fig. 3 Histogram of simulated and observed brightness temperatures from channel 1 to 5. The histograms of land and sea are computed separately for windows channels.

standard deviation in the selected domain normalised to the reference dataset (represented by the radius of the circle centered on the referential origin), the correlation between the selected and reference dataset (represented by the radius with respect to the y-axis), the root mean square error versus the reference dataset (represented by the circles centered on 1 on the x-axis), and the magnitude and sign of the bias (difference between mean simulated and observed brightness temperatures, arrows). Water vapour channels ($BT3-5$) show similar results over land and sea (Fig. 2). The correlation mainly ranges between 0.7 (autumn-winter) and 0.9 (summer). The root mean square errors range from 0.5 to 0.7 K. The standard deviation, i.e., the simulations variability, is half of the observations variability and is slightly larger in summer than in autumn. Finally, the bias is negative: the simulated brightness temperatures are on average lower than the observed ones. Regarding window channels ($BT1-2$), Figure 2 shows a large difference between land and sea in particular in terms of bias, negative for sea and close to zero over land. In terms of variability, the standard deviation for channel 1 is about 0.25 K over the sea and 1 K over land. The correlation for channel 1 is 0.5 over the sea and 0.7 over land. For channel 2, it is between 0.6 and 0.7, independently of the surface characteristics. Globally, the correlation is lower in summer than in other seasons (except for channel 1 over land). Eventually, the root mean square error is slightly higher over land than over the sea for channel 1. Note that, contrarily to the water vapour channels, the brightness temperatures in summer season are less accurately simulated by the model than in other seasons.

The histograms of simulated and observed brightness temperatures (Fig. 3) allow to go a step further in the analyses. Firstly, histograms unravel a higher variability of observed brightness temperatures than of simulated brightness temperatures, in particular for low brightness temperatures. The model does not succeed in simulating high brightness temperatures for water vapour channels. It also underestimates the frequency of low brightness temperatures for all channels. It further fails in simulating very low brightness temperatures. Regarding the window channels, average temperatures are higher over land than over the sea (especially for channel 1) because of the difference in surface properties between land and sea. The difference between land and sea is weaker for channel 2 which is less sensitive to surface properties. The range of brightness temperatures for water vapour channels 3 and 4 is much wider in the observations (140 to 305 K) than in the simulations (180 to 280 K). Moreover the simulated brightness temperatures for water vapour channels 3 and 4 show an abrupt step in brightness temperatures distribution around 230 K.

If the difference for high brightness temperatures between the observations and the simulations looks like a simple shift, the difference for low tem-

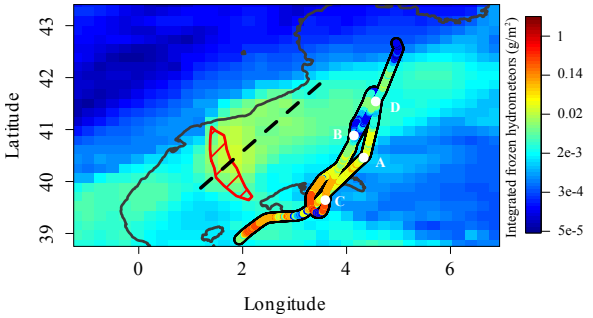

Fig. 4 Integrated frozen hydrometeors content from model (at 12:00) and RASTA radar on 12 October 2012 from (11:55 to 13:50 UTC). The red dashed region shows the convective rainfall from model with rain rate higher than 10 mm/3 h. A vertical cross-section is computed along the black dashed line. The Spanish eastern coast and the Balearic Islands are plotted in black. White letters are used in Figure 5 as points of reference.

peratures appears to be related to an improper simulation of some atmospheric properties, possibly the underestimation of the frozen hydrometeors content. It is interesting to note that the brightness temperatures simulated for channel 5, that probes deeper in the atmosphere, appear more realistic than those simulated for channels 3 and 4 that probe higher in the atmosphere. This suggests the underestimation of frozen hydrometeors could be more significant in mid to high troposphere than in low troposphere.

4 Sensitivity of the simulated brightness temperatures to the frozen hydrometeors

The 12 October 2012 was characterised by the development of convective cells over the Balearic Islands (Fig. 4). RASTA radar detected high integrated frozen hydrometeor content (up to 2.5 g/m^2) both on the southern and northern parts of the Majorca island. The simulation produces convective rainfall along the Spanish eastern coast. Although the simulated convective cell is not strictly identical to the observed one, it developed in a similar large scale environment and is thus expected to produce a similar frozen hydrometeors profile. However, within this convective region, the simulation produces a rather low content of integrated frozen hydrometeors with a maximum of 0.025 g/m^2 at about 1.8 ° E, 40.5 ° N.

Figure 5 shows a vertical cross section of frozen hydrometeors content from the model along a line indicated in Figure 4 and the frozen hydrometeor retrieved by the RASTA radar interpolated at the model resolution. There are two regions with

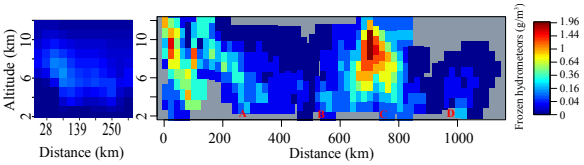

Fig. 5 Vertical cross-section of frozen hydrometeors content from the model (along the black dashed line of Figure 4) (left) and from interpolated (right) RASTA radar observations (along the RASTA track). Letters along the RASTA observations axis correspond to those in Figure 4.

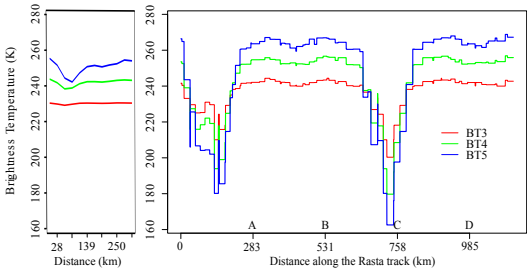

Fig. 6 Simulated brightness temperature of channel 3-5 for model along the black dashed line of Figure 4 (left) and MHS brightness temperatures from NOAA 18 satellite at 13:12 UTC on 12 October 2012 for gridpoints that are the closest to the RASTA flight track (right).

high frozen content along the RASTA path from 0 to 30 km with frozen hydrometeor content higher than 1 g/m^3 between 8 and 11 km height, and from 630 to 780 km with frozen hydrometeor content higher than 0.64 g/m^3 from 5 km to 12 km height (a more detailed analysis of this second system can be found in Rysman et al (2015)). Regarding the simulation, the frozen hydrometeor (solid precipitation and cloud ice) content is higher than 0.04 g/m^3 from 4 to 9 km height with a maximum around 0.16 g/m^3 at 7 km (kilometer 84). Therefore, the model simulates much less frozen hydrometeor than the observations, at least by a factor of 5 in the mid-troposphere. Figure 5 also shows that the median altitude of the maximum of frozen hydrometeor content is lower in the model (7 km) than in the observations (9-10 km).

The altitude and the density of frozen hydrometeors impact the brightness temperature measured by microwave radiometers as explained in the Section 2. The obvious next step is therefore to highlight the impact of the frozen hydrometeors underestimation on brightness temperatures. We thus compared the simulated brightness temperatures along the same cross-section with the observed brightness temperature measured by the MHS sounder along the RASTA track (Fig. 6). The difference is striking; observations show a strong depression for

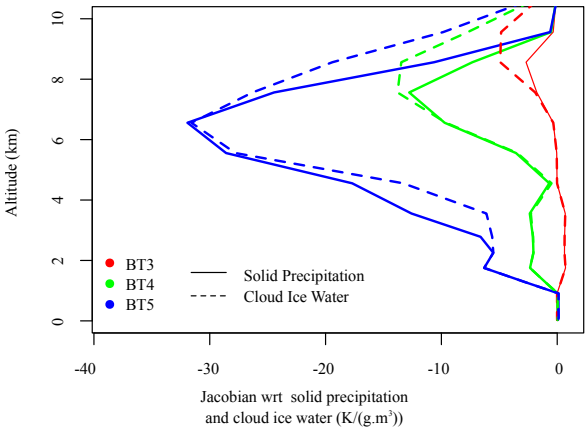

Fig. 7 Jacobian with respect to solid precipitation content (solid line) and cloud ice (dashed line) as a function of altitude. The Jacobian is computed at the grid point with the highest frozen hydrometeors content in the model (i.e., kilometer 84 in Figure 6).

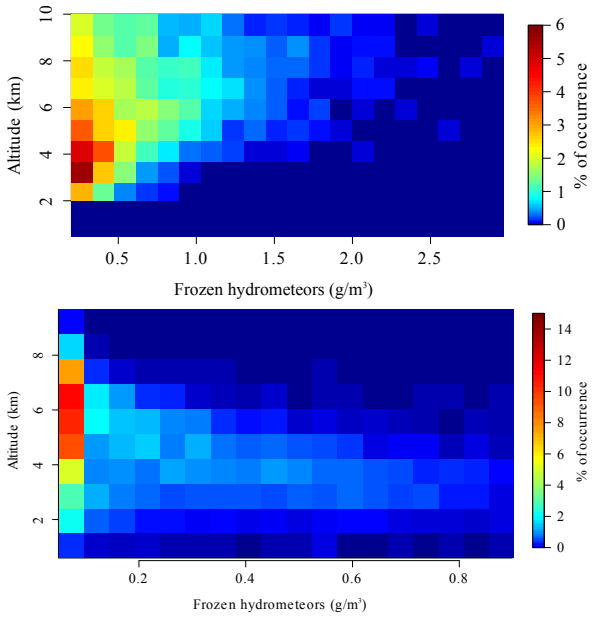

Fig. 8 Percentage of occurrence of frozen hydrometeors versus altitude for RASTA observations (top) and model (bottom) during the HyMeX SOP-1.

the three water vapour channels over the region of high frozen hydrometeors content, while in the simulation only channels 4 and 5, which probes the deepest in the atmosphere, shows a slight decrease over the region with the highest frozen hydrometeors content. The difference in brightness temperature for channel 5 between the region with the highest frozen hydrometeors content and the region without hydrometeors is about 100 K in the observations while it is lower than 15 K in the simulation. This is, at least partially, due the lower content of frozen hydrometeors in the simulation. Moreover, the brightness temperature from channel 3 that probes the highest in the atmosphere, is not depressed at all in the simulation. This is probably because frozen hydrometeors are simulated only at low altitude (Fig. 5).

The microphysics scheme of Hong et al (2004) produces two types of frozen hydrometeors: snow (i.e., solid precipitation) and ice crystals (i.e., cloud ice). In order to evaluate the sensitivity of the simulated brightness temperature on the type of frozen hydrometeors along the vertical in convective cells, we computed the Jacobian of the simulated brightness temperatures with respect to solid precipitation and cloud ice (Fig. 7) at the grid point with the highest frozen hydrometeors content in the simulation (i.e., kilometer 84 in Figure 6). The Jacobian shows that an increase of solid precipitation and cloud ice leads to a decrease of brightness temperatures from 1 km for channel 5, from 4 km for channel 4 and from 7 km for channel 3. For solid precipitation, the Jacobian reaches its minimum at 6.5 km for channel 5 (-32 K.g^{-1}.m^{-3}), at 7 km for channel 4 (-12 K.g^{-1}.m^{-3}) and at 8 km for channel 3 (-3 K.g^{-1}.m^{-3}). The Jacobian is very similar for cloud ice, yet it peaks at higher levels than solid precipitation for channels 3 and 4.

In order to understand if the improper simulation of frozen hydrometeors is systematic, we evaluate the average content and altitude of frozen hydrometeors for the 18 RASTA flights that took place during the HyMeX SOP-1 campaign. Figure 8 highlights that the frozen hydrometeors content and altitude are underestimated during the entire HyMeX SOP-1 (and most probably during the entire 2002-2012 period). The observations show rather high frozen hydrometeors content (up to 2.2 g.m^{-3}). The maximum occurrence of observed frozen hydrometeors, for observations, is found between 3 and 5 km and the highest content in hydrometeors is found in average around 7 km. A relatively high density of frozen hydrometeors is found up to 10 km. The simulated frozen hydrometeors show much lower content in the simulation (mostly lower than 0.3 g.m^{-3}). The maximum of occurrence of frozen hydrometeors content is found higher than the observations (about 6 km) but the highest content of frozen hydrometeors is found around 3.5 km, at lower altitude than in the observations. Moreover, very few frozen hydrometeors are found higher than 8 km. Note that Figure 8 shows simulated solid precipitation and cloud ice together; cloud ice alone shows content about 5 times inferior to solid precipitation (not shown).

5 Sensitivity of the simulated brightness temperatures to the ice particle shape

In previous sections, we simulated brightness temperatures using the setting suggested by Geer and Baordo (2014) for the scattering of frozen hydrometeors in RTTOV. However, this setting has been established for different conditions that the ones considered in this study. Therefore, we tested here the sensitivity of the brightness temperatures simulation to the RTTOV setting, independently of the, already highlighted, issue of the underestimation of the frozen hydrometeors in the simulation. The scattering of hydrometeors simulated in RTTOV can be tuned by representing frozen hydrometeors as spheres with variable densities. However it has been shown that, when using Mie spheres to represent frozen hydrometeors, realistic brightness temperatures can not be simulated at all microwave frequencies. In particular, this approach leads to overestimated scattering for middle frequencies (30-50 GHz) and underestimated scattering at high frequencies (150-183 GHz) (Kim et al, 2007; Geer and Baordo, 2014; Guerbette et al, 2016). Moreover, spheres are particularly unrealistic shapes for frozen hydrometeors. Another option available in RTTOV consists in representing frozen hydrometeors as three-dimensional snowflakes/ice crystals using the discrete dipole approximation. Such shapes are more physically meaningful and succeed in simulating realistic scattering at all microwave frequencies (Geer and Baordo, 2014).

In the following, we tested, for the 12 October 2012 case, the sensitivity of brightness temperatures to the 11 ice particle shapes listed in Table 1 in Liu (2008) (e.g., Short Column, 3-Bullet Rosette, and Sector Snowflake) and to the Mie sphere. We also increased the solid precipitation content by a factor of 5 in order to obtain a more realistic frozen hydrometeors content in the mid-troposphere (see previous section). It is important to note that none of the ice particle shape tested leads to a realistic brightness temperature depression without increasing the frozen hydrometeors content in the WRF simulation.

Tests reveal that the "Thin Plate" ice particle shape is the one that best matches the simulated convective rainfall area (Figure 9, red dashed region) and shows a realistic brightness temperatures depression compared to MHS measurements. Using this shape, the depression of brightness temperature from channel 5 reaches -70 K above the convective region of the cell compared to clear sky

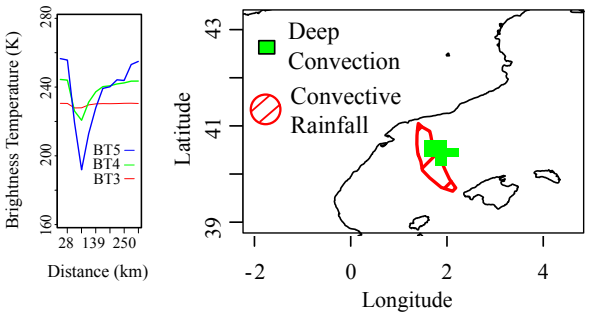

Fig. 9 (left) Simulated brightness temperature of channel 3-5 for model along the black dashed line of Figure 4 and (right) convective rainfall (red) and deep convection diagnostics from simulated brightness temperatures using "Thin Plate" ice particles shape and solid precipitation increased by a factor of 5 (green).

Block Column	153 K
Short Column	158 K
Thick Plate	163 K
Long Column	173 K
Mie Sphere 900 kg/m^3	190 K
Thin Plate	192 K
3-Bullet Rosette	215 K
Mie Sphere 400 kg/m^3	217 K
Sector Snowflake	220 K
5-Bullet Rosette	239 K
6-Bullet Rosette	239 K
4-Bullet Rosette	240 K
Dendrite Snowflake	242 K
Mie Sphere 100 kg/m^3	244 K

Table 1 Lowest brightness temperature over the convective region shown in Figure 9 simulated for channel 5 for several tested ice particle shapes. Note the solid precipitation is increased by a factor of 5 in the WRF simulation.

conditions. Channel 4 brightness temperature depression is nearly -25 K in this region. Note that brightness temperature from channel 3 does not show any significant depression because the frozen hydrometeor content in the high troposphere is very low compared to observations, even if multiplied by 5. Figure 9 shows that the area where deep convection is diagnosed from simulated brightness temperatures (green) only partially overlaps the convective rainfall region (red). The diagnostic is not fulfilled at the edge of the convective rainfall area, but is fulfilled at the rear of the cell (northeastern of the convective rainfall area) where frozen hydrometeors show high density (Fig. 4).

Amongst the other tested ice particle shapes, "Short Column", "Block Column" and "Thick Plate" tend to produce strong brightness temperatures

depression (Table 1) but strongly overestimate the deep convection region (not shown). "Long Column" produces a realistic brightness temperature depression compared to Figure 6 but overestimates the deep convection area (not shown). Other shapes moderately ("3-Bullet Rosette" and "Sector Snowflake") or strongly ("4-Bullet Rosette", "5-Bullet Rosette", "6-Bullet Rosette", and "Dendrite Snowflake") underestimate the scattering by frozen hydrometeors. It might sound unphysical that the shape that leads to the more realistic brightness temperatures in our simulation is the "Thin Plate" whereas the simulation only produces snow. In fact, it illustrates that only the presence of ice particles such as hail can explain the significant observed brightness temperature depression of the 12 October 2012 case (Fig. 6). Note that although we privileged the more physical shape of "Thin Plate", it was also possible to simulate realistic brightness temperature depression using Mie spheres but it required a particularly high density of at least 900 kg/m^3 (density of aggregate).

6 Evaluation of simulated rainfall

This last section is dedicated to the evaluation of the total and convective rainfall simulated by the model. To this end, we compared the occurrence of simulated total and convective rainfall with the rainfall and the deep convection occurrence derived from (i) the observed and (ii) the simulated brightness temperatures (see Section 2). We used the "Thin Plate" ice particle shape to compute the brightness temperatures as a result of the sensitivity test described above. The rainfall diagnostic performs poorly for a cold surface under clear sky conditions (Funatsu et al, 2008) which can be found in winter and/or for elevated altitudes in the Mediterranean region. The comparison is thus conducted for spring, summer and autumn seasons and for altitudes below 1700 m (except in summer). In addition, as explained in the Section 2, the rainfall diagnostic method mainly detects rain events with rain rate greater than 10 mm/3h. Therefore, we retained the occurrences of precipitation with rain rate higher than 10 mm/3h in WRF. Finally, in the following, "WRF" rain (resp. convection) refers to rainfall (resp. convective rainfall) simulated by the WRF model while "WRF-RTTOV" rain (resp. convection) refers to rainfall (resp. convection) diagnosed from simulated brightness temperatures.

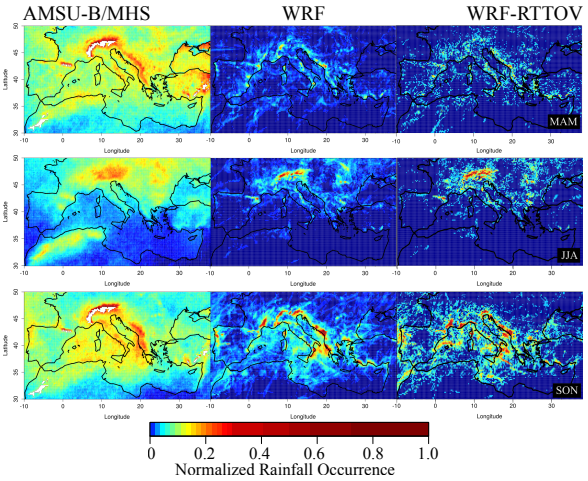

Fig. 10 Rainfall occurrence according to AMSU-B/MHS (%) (left), WRF (rain rate higher than 10 mm/3 h (%) (middle), and WRF-RTTOV (rain diagnosed from simulated brightness temperatures) (%) with solid precipitation content multiplied by 5 in convective region (right).

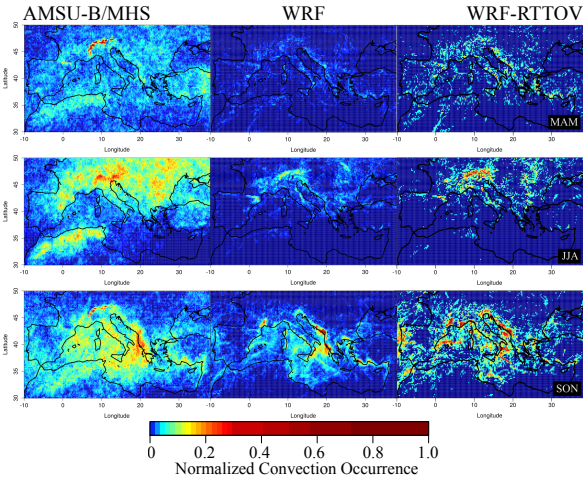

Fig. 11 Deep convection occurrence according to AMSU-B/MHS (%) (left), WRF (convective rainfall with rain rate higher than 10 mm/3 h) (%) (middle), and WRF-RTTOV (DC diagnosed from simulated brightness temperatures) (%) with solid precipitation content multiplied by 5 in convective region (right).

The main difference between AMSU-B/MHS and WRF ((Fig. 10), left and middle panels) lies in the widespread distribution of rainfall in the observations while large areas inland and over the sea are dry in the simulations. Overall, there is a good agreement in the seasonal cycle between both datasets: in spring (MAM), precipitation is mainly located over the sea, on the northern coasts (especially in mountainous regions) and over the Atlas. In summer (JJA), rain occurs in European land with many occurrences in mountainous areas. In autumn (SON), the pattern is rather sim-

ilar to MAM although with more frequent occurrences of rain, especially over the sea and in the Balkans. However, there are some discrepancies between AMSU-B and WRF precipitation such as the lack of simulated occurrences over the Black Sea and Northern Turkey in spring, in the Atlas in summer and in the Southwestern Mediterranean in autumn. AMSU-B/MHS does not show some gridpoint maxima of occurrences that are present in the simulation in the regions of Valencia (Spain), the Cévennes (France), Corsica, Calabria (Italy), Eastern Greece and in Portugal in autumn and in Eastern Spain in spring.

Regarding convection (Fig. 11) (left and middle), once again the occurrences are much more widespread in the observations than in the simulation. Although the seasonal cycle is quite similar between the observations and the simulation, large discrepancies exist in particular in spring when very few convective events occur in the simulation. In greater details, in spring, convection is found equally over land and over the sea in observations and only along the northern Mediterranean coast in simulation. In summer, AMSU-B/MHS convection occurs over land for latitude higher than 43 $^\circ$ N with a maximum in Northern Italy and also in the Atlas. The same maximum of convection in Northern Italy is found in WRF convection. However, convection is missing in the Atlas region in WRF. In autumn, convection moves towards the Mediterranean Sea with maxima along the Eastern Adriatic coast. In this season, AMSU-B/MHS and WRF convection show rather similar patterns, yet the former shows once again more widespread occurrences. It is also interesting to note that spring precipitation seems less related to deep convection than summer and autumn precipitation, both in AMSU-B/MHS observations and the simulation.

The obvious last step of this analysis is to evaluate the rain and deep convection diagnosed from simulated brightness temperatures. However, when applying the rain and deep convection diagnostics to simulated brightness temperatures, hardly any rain and deep convection is detected. Nevertheless, we showed that the underestimation of solid precipitation by a factor of 5 in the simulation (Fig. 8) impacts the simulated brightness temperatures (Fig. 7). Therefore, we investigate the effect of an increase in solid precipitation content on the validity of both rainfall and deep convection diagnostics. Specifically, we increased by a factor of 5 the solid precipitation content of every model output for which convective rainfall is detected. Then, we recomputed the brightness temperature and checked again the rain and deep convection occurrence diagnostics. Note that the original solid precipitation content is used for WRF rainfall and convection (middle column of Figure 10 and Figure 11).

Results show that WRF-RTTOV rainfall and convection (with the solid precipitation multiplied by 5) are quite similar to WRF rainfall and convection, respectively. The main differences are that WRF-RTTOV rainfall and convection occurrences are more scattered and that more convection in found in spring for WRF-RTTOV than for WRF.

7 Summary and discussion

This study aims at assessing the potential of passive microwave observations to evaluate decadal simulations of regional climate models. The evaluation is conducted on a simulation covering the period 2002-2012 at 3-h and 20 km resolutions over the Mediterranean region (land and sea) using a model-to-satellite approach. Specifically, we simulate brightness temperatures from the Weather and Research Forecasting (WRF) 3-hourly model outputs using the radiative transfer model RTTOV (v11). Simulated brightness temperatures show a correlation of 0.8 with observed brightness temperatures for water vapour channels. The correlation is lower for window channels especially over sea for the 89 GHz channel ($\sim$0.5). The observed brightness temperature values show a higher variability than the simulated ones. In particular, the most striking discrepancy between the simulation and the observations lies in the improper simulation of very low brightness temperatures. Since low brightness temperatures are usually associated with the scattering from frozen hydrometeors at high microwave frequencies, we evaluate the simulated frozen hydrometeors loading using observations from the airborne RASTA radar. Results showed that the frozen hydrometeors content is underestimated by the model (at least by a factor of 5) and that the median altitude of frozen hydrometeors is lower in the simulation than in the observations. Thereafter, we seek for the most appropriate ice particle shape for simulating scattering by frozen hydrometeors with RTTOV in the conditions of this study. Tests show that the "Thin Plate" ice particle shape produces the most consistent brightness temperatures compared to observations in the studied convective system. Then, we

evaluate the simulated rainfall occurrence and distribution. If the simulated rainfall matches reasonably well the observed rainfall, hardly any rainfall is detected when directly diagnosed from the simulated brightness temperatures. However, when simulated solid precipitation is increased by a factor of 5 in convective regions, rainfall diagnosed from simulated brightness temperatures is much more in agreement with the observations.

These results illustrate the potential but also the present limitations of using passive microwave observations for the evaluation of precipitating systems in regional models. AMSU-B/MHS instruments are available since 1999, on-board several platforms, and have fair spatial and temporal resolutions. They should thus be particularly well designed for the evaluation of long-term simulations of regional models. However, if a comparison of WRF and AMSU-B/MHS products is straightforward and useful as a first step (Claud et al, 2012), the use of a model-to-satellite approach is more problematic as it relies on the combined performance of a climate model (here WRF) and a radiative transfer model (RTTOV).

Regarding the climate model, as microwave measurements are highly sensitive to every atmospheric water component (water vapour, rain, frozen hydrometeors, etc.), the accurate simulation of brightness temperatures requires the model to reproduce consistently and accurately every component of the atmospheric water. In the present study, the model simulates a rainfall occurrence spatial distribution consistent with the observations because parameterizations are well chosen for this purpose. As a matter of fact, most of the evaluation of this simulation has been conducted for precipitation (Flaounas et al, 2013; Lebeaupin Brossier et al, 2015; Berthou et al, 2014, 2015; Lebeaupin-Brossier et al, 2015; Berthou et al, 2016) products. However, the outputs available from the simulation do not provide realistic frozen hydrometeors content. A more realistic frozen hydrometeors content and vertical distribution would not only lead to more realistic brightness temperatures but also, since solid and liquid precipitation are intrinsically related (e.g., Field and Heymsfield (2015); Mülmenstädt et al (2015)), to a possible improvement of the overall simulation of rainfall.

The underestimation of the frozen hydrometeors in the simulation assessed in this paper could have multiple causes. Firstly, it can be related to the microphysics scheme (WRF Single-Moment 5-class microphysical parameterization (Hong et al, 2004)). In particular, this microphysics scheme does not include high density frozen precipitating hydrometeors (such as graupel and aggregate) that strongly scatter radiation and depress observed brightness temperatures. Another issue lies in the treatment of hydrometeors in convection. The microphysics scheme provides an estimation of the frozen hydrometeors only from large-scale precipitating events while information about the sub-grid hydrometeors is provided through the convection scheme (Kain-Fritsch scheme in the present study). This scheme estimates the mass fluxes from which it is possible to derive hydrometeors. However, the sole sub-grid rainfall has been computed for this simulation and the mass flux variable, from which we could have inferred the frozen hydrometeors content, is not available with this simulation as it is not a standard output required by the MED-CORDEX program. Surely, adding frozen hydrometeors derived from the mass flux will help reach more realistic simulations of the ice frozen hydrometeors. We thus urge the upcoming MED-CORDEX programs to provide the mass flux variable as a standard output of simulations. Another approach could be to simulate brightness temperatures in real-time at the model time-step and to provide brightness temperatures as a standard output of the simulations.

In order to simulate more realistic brightness temperatures, we multiplied solid precipitation by 5, which led to a more consistent rainfall spatial distribution. Obviously, such a basic method can have numerous side effects and does not account for the incorrect simulation of the altitude of solid precipitation. Therefore, improvement of simulations requires to identify the suited convective and microphysics schemes and to develop more interactions between both schemes. This could be done following the work of Piriou et al (2007) who developed convection parameterization with separated subgrid microphysics and transport terms. The resolution used in the simulations, i.e., 28 vertical levels and 20 km horizontally, and in most long-term regional model simulations is also problematic, being simply not high enough to resolve fine scale convective processes leading to potential underestimation of frozen hydrometeors by the model. The development of convection-permitting models at a regional scale on long-term periods (Kendon et al, 2012; Prein et al, 2015) may overcome this problem by directly resolving hydrometeors generated by convection with the microphysics scheme.

Interestingly, Wu et al (2015) recently conducted WRF simulations at 0.2 ° horizontal resolution with 50 levels in the vertical over the central and eastern Pacific. They evaluated five convective parameterizations together with the WRF single-moment 6-class microphysics scheme that produces high density frozen hydrometeors. Similarly to our analysis, they highlighted precipitation is well simulated in the model but ice clouds are underestimated for all convective parameterizations.

Our results suggest that improving the simulation of frozen hydrometeors by the model will greatly increase the interest of using model-to-satellite approach to evaluate regional model simulations. Further improvements will come from the RTTOV radiative transfer model. In particular, regarding the specific problem of radiation scattering by frozen hydrometeors, further efforts are needed to take into account the variety of shape of ice particles (rather than one identical shape for every frozen hydrometeor) that will lead to more physical scattering. A first step will be to allow the use of graupel and aggregate frozen particles in the RTTOV-SCATT module. It could be also relevant and physically meaningful to use a different ice particle shape depending on the surface properties and the atmospheric condition. For instance, Geer and Baordo (2014) showed the "Thin Plate" and "Block Column" shape are the best choice for regions of convective snow over land but it is the "Sector Snowflake" shape that produces the most realistic brightness temperatures in average elsewhere. Other improvements will be possible by taking into account the preferential orientation of large particles and by a better representation of the particle size distribution. This is also why measurements campaign such as HyMeX are essential. For instance, during this campaign, airborne in-situ measurements of ice particle have been conducted that help improve our knowledge of the frozen microphysics in the Mediterranean region. In particular, it highlighted the extremely high variability and the complexity of frozen hydrometeors shape, size, distribution (Fontaine et al, 2013).

In this study, we only presented the results for runs in atmosphere-only mode because the results are very similar to those of the atmosphere-ocean coupled mode. Lebeaupin-Brossier et al (2015) show that the main difference between these two twin simulations is the spatial redistribution of rain over the Mediterranean. Yet, we showed that the frozen hydrometeors associated with rainfall are missing or that there are too few of them in the simulation and thus the brightness temperatures for water vapour channels are not correctly simulated. As a consequence, the difference in precipitation distribution does not affect the overall comparison between the observations and the simulation. Improving the simulation of frozen hydrometeors may lead to greater differences between the atmosphere-only and atmosphere-ocean coupled simulations.

Acknowledgements We would like to acknowledge Karine Béranger and Aurélien Podglajen for their insightful comments. We would also like to acknowledge the three referees for their careful proofreading of this paper and their appreciated suggestions that greatly improved this study. This work is a contribution to the HyMeX program (Hydrological cycle in The Mediterranean eXperiment) through INSU-MISTRALS support and the Med-CORDEX program (COordinated Regional climate Downscaling EXperiment Mediterranean region). This study was sponsored by the Direction Générale de l'Armement (PRECIP-CLOUD project), Earth2Observe project (funding from the European Union's Framework Programme under grant agreement number 603608), the ANR-14-CE01-0014 MUSIC project, the ANR-12-SENV-001 REMEMBER project, the ANR-11-BS56-0005 IODA-MED project and the Centre National d'Études Spatiales (CNES). It was also supported by the IPSL group for regional climate and environmental studies, with granted access to the HPC resources of IDRIS (under allocation i2011010227). The authors acknowledge the HyMeX database teams (ESPRI/IPSL and SEDOO/Observatoire Midi-Pyrénées), the French Mixed Service Unit project ICARE/climserv and the MED-CORDEX database team at ENEA for their help in accessing the data (AMSU-B and MHS data, RASTA data and the IPSL WRF and MORCE regional climate simulations). It is also a contribution to the cross-cutting activity on sub-daily precipitation of the GEWEX program of the World Climate Research Program (WCRP) (GEWEX Hydroclimate Panel).

References

Aires F, Prigent C, Bernardo F, Jiménez C, Saunders R, Brunel P (2011) A tool to estimate land-surface emissivities at microwave frequencies (telsem) for use in numerical weather prediction. Quarterly Journal of the Royal Meteorological Society 137(656):690–699

Argence S, Lambert D, Richard E, Chaboureau JP, Söhne N (2008) Impact of initial condition uncertainties on the predictability of heavy rainfall in the mediterranean: a case study. Quarterly Journal of the Royal Meteorological Society 134(636):1775–1788

Barkhordarian A, von Storch H, Bhend J (2013) The expectation of future precipitation change over the mediterranean region is different from what we observe. Climate Dynamics 40(1-2):225–244

Bennartz R, Bauer P (2003) Sensitivity of microwave radiances at 85–183 ghz to precipitating ice particles. Radio Science 38(4)

Bennartz R, Petty GW (2001) The sensitivity of microwave remote sensing observations of precipitation to ice particle size distributions. Journal of Applied Meteorology 40(3):345–364

Berthou S, Mailler S, Drobinski P, Arsouze T, Bastin S, Béranger K, Lebeaupin-Brossier C (2014) Prior history of mistral and tramontane winds modulates heavy precipitation events in southern france. Tellus A 66

Berthou S, Mailler S, Drobinski P, Arsouze T, Bastin S, Béranger K, Lebeaupin-Brossier C (2015) Sensitivity of an intense rain event between atmosphere-only and atmosphere–ocean regional coupled models: 19 september 1996. Quarterly Journal of the Royal Meteorological Society 141(686):258–271

Berthou S, Mailler S, Drobinski P, Arsouze T, Bastin S, Béranger K, Flaounas E, Lebeaupin Brossier C, Stéfanon M (2016) Influence of submonthly air-sea coupling on heavy precipitation events in the western mediterranean basin. Quarterly Journal of the Royal Meteorological Society DOI 10.1002/qj.2717

Bonsignori R (2007) The Microwave Humidity Sounder (MHS): in-orbit performance assessment. In: Society of Photo-Optical Instrumentation Engineers (SPIE) Conference Series, Society of Photo-Optical Instrumentation Engineers (SPIE) Conference Series, vol 6744, p 0, DOI 10.1117/12.737986

Bouniol D, Protat A, Plana-Fattori A, Giraud M, Vinson JP, Grand N (2008) Comparison of Airborne and Spaceborne 95-GHz Radar Reflectivities and Evaluation of Multiple Scattering Effects in Spaceborne Measurements. Journal of Atmospheric and Oceanic Technology 25:1983, DOI 10.1175/2008JTECHA1011.1

Bresson E, Ducrocq V, Nuissier O, Ricard D, de Saint-Aubin C (2012) Idealized numerical simulations of quasi-stationary convective systems over the northwestern Mediterranean complex terrain. Quarterly Journal of the Royal Meteorological Society 138(668):1751–1763, DOI 10.1002/qj.1911

Burns B, Wu X, Diak GR, et al (1997) Effects of precipitation and cloud ice on brightness temperatures in amsu moisture channels. Geoscience and Remote Sensing, IEEE Transactions on 35(6):1429–1437

Casella D, Panegrossi G, Sano P, Dietrich S, Mugnai A, Smith E, Tripoli GJ, Formenton M, Di Paola F, Leung WYH, et al (2013) Transitioning from crd to cdrd in bayesian retrieval of rainfall from satellite passive microwave measurements: Part 2. overcoming database profile selection ambiguity by consideration of meteorological control on microphysics. Geoscience and Remote Sensing, IEEE Transactions on 51(9):4650–4671

Chaboureau JP, Söhne N, Pinty JP, Meirold-Mautner I, Defer E, Prigent C, Pardo JR, Mech M, Crewell S (2008) A midlatitude cloud database validated with satellite observations. J Appl Meteor Climatol 47:1337–1353, DOI 10.1175/2007JAMC1731.1

Chakroun M, Bastin S, Chiriaco M, Chepfer H (2016) Characterization of vertical cloud variability over europe using spatial lidar observations and regional simulation. Climate Dynamics pp 1–23

Clark H, Chaboureau JP (2010) Uncertainties in short-term forecasts of a Mediterranean heavy precipitation event: Assessment with satellite observations. Journal of Geophysical Research 115:D22213, DOI 10.1029/2010JD014388

Claud C, Alhammoud B, Funatsu BM, Lebeaupin Brossier C, Chaboureau JP, Béranger K, Drobinski P (2012) A high resolution climatology of precipitation and deep convection over the Mediterranean region from operational satellite microwave data: development and application to the evaluation of model uncertainties. Natural Hazards and Earth System Sciences 12:785–798, DOI 10.5194/nhess-12-785-2012

Dee DP, Uppala SM, Simmons AJ, Berrisford P, Poli P, Kobayashi S, Andrae U, Balmaseda MA, Balsamo G, Bauer P, Bechtold P, Beljaars ACM, van de Berg L, Bidlot J, Bormann N, Delsol C, Dragani R, Fuentes M, Geer AJ, Haimberger L, Healy SB, Hersbach H, Hlm EV, Isaksen L, Kllberg P, Khler M, Matricardi M, McNally AP, Monge-Sanz BM, Morcrette JJ, Park BK, Peubey C, de Rosnay P, Tavolato C, Thpaut JN, Vitart F (2011) The ERA-Interim reanalysis: configuration and performance of the data assimilation system. Quarterly Journal of the Royal Meteorological Society 137(656):553–597, DOI 10.1002/qj.828

Deeter M, Vivekanandan J (2005) Amsu-b observations of mixed-phase clouds over land. Journal of applied meteorology 44(1):72–85

Defer E, Prigent C, Aires F, Pardo JR, Walden CJ, Zanif OZ, Chaboureau JP, Pinty JP (2008) Development of precipitation retrievals at millimeter and submillimeter wavelengths for geostationary satellites. Journal of Geophysical Research 113:D08,111, doi:10.1029/2007JD008,673

Delanoë J, Protat A, Bouniol D, Heymsfield A, Bansemer A, Brown P (2007) The Characterization of Ice Cloud Properties from Doppler Radar Measurements. Journal of Applied Meteorology and Climatology 46:1682, DOI 10.1175/JAM2543.1

Delanoë J, Protat A, Jourdan O, Pelon J, Papazzoni M, Dupuy R, Gayet JF, Jouan C (2013) Comparison of Airborne In Situ, Airborne Radar-Lidar, and Spaceborne Radar-Lidar Retrievals of Polar Ice Cloud Properties Sampled during the POLARCAT Campaign. Journal of Atmospheric and Oceanic Technology 30:57–73, DOI 10.1175/JTECH-D-11-00200.1

Delanoë J, Heymsfield AJ, Protat A, Bansemer A, Hogan RJ (2014) Normalized particle size distribution for remote sensing application. Journal of Geophysical Research (Atmospheres) 119:4204–4227, DOI 10.1002/2013JD020700

Drobinski P, Anav A, Lebaupin-Brossier C, Samson G, Stéfanon M, Bastin S, Baklouti M, Béranger K, Beuvier J, Bourdallé-Badie R, Coquart L, D'Andrea F, De Noblet-Ducoudr N, Diaz F, Dutay J, Ethe C, Foujols M, Khvorostyanov D, Madec G, Mancip M, Masson S, Menut L, Palmieri J, Polcher J, Turquety S, Valcke S, Viovy N (2012) Modelling the regional coupled earth system (morce): Application to process and climate studies in vulnerable regions. Environmental Modelling & Software 35:1–18

Drobinski P, Ducrocq V, Alpert P, Anagnostou E, Borga M, Braud I, Chanzy A, Delrieu G, Estournel C, Boubrahmi NF, Font J, Grubisic V, Gualdi S, Kottmeier C, Kotroni V, Lagouvardos K, Lionello P, Llasat MC, Ludwig W, Lutoff C, Mariotti A, Richard E, Romero R, Rotunno R, Roussot O, Ruin I, Tintore J, Uijlenhoet R, Wernli H (2014) HyMeX, a 10-year multidisciplinary program on the Mediterranean water cycle. Bulletin of the American Meteorological Society 5(24)

Ducrocq V, Nuissier O, Ricard D, Lebeaupin C, Thouvenin T (2008) A numerical study of three catastrophic precipitating events over southern France. II: mesoscale triggering and stationarity factors. Quarterly Journal of the Royal Meteorological Society 134(630):131–145, DOI 10.1002/qj.199

Ducrocq V, Braud I, Ferretti R, Davolio S, Flamant C, Jansa A, Kalthoff N, Taupier-letage I, Ayral Pa, Berne A, Borga M, Boudevillain B, Boichard Jl, Bousquet O, Bouvier C, Chiggiato J, Cimini D, Coppola L, Cocquerez P, Defer E, Girolamo PD, Doerenbecher A, Dufournet Y, Gourley JJ, Labatut L, Lambert D, Frank S, Montani A, Nord G, Nuret M, Ramage K, Rison B, Roussot O, Schwarzenboeck A, Testor P, Tamayo J (2014) HyMeX-SOP1, the field campaign dedicated to heavy precipitation and flash flooding in the northwestern Mediterranean. Bulletin of the American Meteorological Society 11:1–59

Dudhia J (1989) Numerical study of convection observed during the winter monsoon experiment using a mesoscale two-dimensional model. Journal of the Atmospheric Sciences 46(20):3077–3107

Duffourg F, Ducrocq V (2011) Origin of the moisture feeding the heavy precipitating systems over southeastern France. Natural Hazards and Earth System Sciences 11(4):1163–1178, DOI 10.5194/nhess-11-1163-2011

Duffourg F, Ducrocq V (2013) Assessment of the water supply to Mediterranean heavy precipitation: a method based on finely designed water budgets: Water supply to HPEs: assessment with water budgets. Atmospheric Science Letters 14(3):133–138, DOI 10.1002/asl2.429

Eyre J (1991) A fast radiative transfer model for satellite sounding systems. European Centre for Medium-Range Weather Forecasts

Ferraro R, Beauchamp J, Cecil D, Heymsfield G (2015) A prototype hail detection algorithm and hail climatology developed with the advanced microwave sounding unit (amsu). Atmospheric Research 163:24–35

Ferraro RR, Weng F, Grody NC, Zhao L (2000) Precipitation characteristics over land from the noaa-15 amsu sensor. Geophysical Research Letters 27(17):2669–2672

Ferraro RR, Weng F, Grody NC, Zhao L, Meng H, Kongoli C, Pellegrino P, Qiu S, Dean C (2005) Noaa operational hydrological products derived from the advanced microwave sounding unit. Geoscience and Remote Sensing, IEEE Transactions on 43(5):1036–1049

Field P, Heymsfield AJ (2015) Importance of snow to global precipitation. Geophysical Research Letters pp n/a–n/a, DOI

10.1002/2015GL065497, 2015GL065497

Field PR, Heymsfield AJ, Bansemer A (2007) Snow size distribution parameterization for midlatitude and tropical ice clouds. Journal of the Atmospheric Sciences 64(12):4346–4365

Flaounas E, Drobinski P, Vrac M, Bastin S, Lebeaupin-Brossier C, Stéfanon M, Borga M, Calvet JC (2013) Precipitation and temperature space–time variability and extremes in the mediterranean region: evaluation of dynamical and statistical downscaling methods. Climate dynamics 40(11-12):2687–2705

Fontaine E, Schwarzenboëck A, Delanoë J, Dupuy R, Leroy D, Duroure C, Gourbeyre C, Fournol JF, Febvre G (2013) Determination of area-diameter and mass-diameter relationships from ice particle imagery in order to deduce iwc within mid- latitude convective clouds observed over the mediterranean basin, 7th HyMeX Workshop, Cassis, France

Funatsu BM, Claud C, Chaboureau JP (2007) Potential of Advanced Microwave Sounding Unit to identify precipitating systems and associated upper-level features in the Mediterranean region: Case studies. Journal of Geophysical Research (Atmospheres) 112(11):D17113

Funatsu BM, Claud C, Chaboureau JP (2008) A 6-year AMSU-based climatology of upper-level troughs and associated precipitation distribution in the Mediterranean region. Journal of Geophysical Research (Atmospheres) 113(12):D15120, DOI 10.1029/2008JD009918

Funatsu BM, Claud C, Chaboureau JP (2009) Comparison between the Large-Scale Environments of Moderate and Intense Precipitating Systems in the Mediterranean Region. Monthly Weather Review 137:3933, DOI 10.1175/2009MWR2922.1

García-Herrera R, Barriopedro D, Hernández E, Paredes D, Correoso JF, Prieto L (2005) The 2001 mesoscale convective systems over iberia and the balearic islands. Meteorology and atmospheric physics 90(3-4):225–243, DOI 10.1007/s00703-005-0114-2

Geer A, Baordo F (2014) Improved scattering radiative transfer for frozen hydrometeors at microwave frequencies. Atmospheric Measurement Techniques 7(6):1839–1860

Gloersen P, Barath FT (1977) A scanning multichannel microwave radiometer for nimbus-g and seasat-a. Oceanic Engineering, IEEE Journal of 2(2):172–178

Guerbette J, Mahfouf JF, Plu M (2016) Towards the assimilation of all-sky microwave radiances from the saphir humidity sounder in a limited area nwp model over tropical regions. Tellus A 68

Haylock M, Hofstra N, Klein Tank A, Klok E, Jones P, M N (2008) A European daily high-resolution gridded dataset of surface temperature and precipitation. Journal of Geophysical Research 113:D20,119, DOI 10.1029/2008JD10201

Hong G, Heygster G, Miao J, Kunzi K (2005a) Detection of tropical deep convective clouds from amsu-b water vapor channels measurements. Journal of Geophysical Research: Atmospheres (1984–2012) 110(D5)

Hong G, Heygster G, Miao J, Kunzi K (2005b) Sensitivity of microwave brightness temperatures to hydrometeors in a tropical deep convective cloud system at 89–190 ghz. Radio science 40(4)

Hong SY, Dudhia J, Chen SH (2004) A revised approach to ice microphysical processes for the bulk parameterization of clouds and precipitation. Monthly Weather Review 132(1):103–120

Houze RA (2004) Mesoscale convective systems. Reviews of Geophysics 42(4), DOI 10.1029/2004RG000150

Jansà A, Genovés A, Picornell M, Campins J, Riosalido R, Carretero O (2001) Western Mediterranean cyclones and heavy rain. part 2: Statistical approach. Meteorological Applications 8(1):43–56

Kain JS (2004) The Kain–Fritsch convective parameterization: An update. Journal of Applied Meteorology 43(1):170–181, DOI 10.1175/1520-0450(2004)043

Karbou F, Aires F, Prigent C, Eymard L (2005) Potential of advanced microwave sounding unit-a (amsu-a) and amsu-b measurements for atmospheric temperature and humidity profiling over land. Journal of Geophysical Research: Atmospheres (1984–2012) 110(D7)

Kendon EJ, Roberts NM, Senior CA, Roberts MJ (2012) Realism of Rainfall in a Very High-Resolution Regional Climate Model. Journal of Climate 25(17):5791–5806, DOI 10.1175/JCLI-D-11-00562.1

Kidd C, Matsui T, Chern J, Mohr K, Kummerow C, Randel D (2016) Global precipitation estimates from cross-track passive microwave observations using a physically based retrieval scheme. Journal of Hydrometeorology

17(1):383–400

Kim MJ, Kulie MS, O'Dell C, Bennartz R (2007) Scattering of ice particles at microwave frequencies: A physically based parameterization. Journal of applied meteorology and climatology 46(5):615–633

Kummerow C, Giglio L (1994) A passive microwave technique for estimating rainfall and vertical structure information from space. part i: Algorithm description. Journal of Applied Meteorology 33(1):3–18

Kummerow C, Hong Y, Olson W, Yang S, Adler R, McCollum J, Ferraro R, Petty G, Shin DB, Wilheit T (2001) The evolution of the goddard profiling algorithm (gprof) for rainfall estimation from passive microwave sensors. Journal of Applied Meteorology 40(11):1801–1820

Laviola S, Levizzani V (2011) The 183-WSL fast rain rate retrieval algorithm: Part I: Retrieval design. Atmospheric Research 99:443–461, DOI 10.1016/j.atmosres.2010.11.013

Lebeaupin-Brossier C, Drobinski P, Béranger K, Bastin S, Orain F (2013) Ocean memory effect on the dynamics of coastal heavy precipitation preceded by a mistral event in the northwestern mediterranean. Quarterly Journal of the Royal Meteorological Society 139(675):1583–1597

Lebeaupin-Brossier C, Bastin S, Béranger K, Drobinski P (2015) Regional mesoscale air–sea coupling impacts and extreme meteorological events role on the mediterranean sea water budget. Climate Dynamics 44(3-4):1029–1051

Lebeaupin Brossier C, Bastin S, Béranger K, Drobinski P (2015) Regional mesoscale air-sea coupling impacts and extreme meteorological events role on the Mediterranean Sea water budget. Climate Dynamics 44:1029–1051, DOI 10.1007/s00382-014-2252-z

Liu G (2008) A database of microwave single-scattering properties for nonspherical ice particles. Bulletin of the American Meteorological Society 89(10):1563–1570

Marzano FS, Mugnai A, Panegrossi G, Pierdicca N, Smith E, Turk J, et al (1999) Bayesian estimation of precipitating cloud parameters from combined measurements of spaceborne microwave radiometer and radar. Geoscience and Remote Sensing, IEEE Transactions on 37(1):596–613

Matricardi M, Chevallier F, Kelly G, Thépaut JN (2004) An improved general fast radiative transfer model for the assimilation of radiance observations. Quarterly Journal of the Royal Meteorological Society 130(596):153–173

Meirold-Mautner I, Prigent C, Defer E, Pardo JR, Chaboureau JP, Pinty JP, Mech M, Crewell S (2007) Radiative transfer simulations using mesoscale cloud model outputs: Comparisons with passive microwave and infrared satellite observations for midlatitudes. Journal of the atmospheric sciences 64(5):1550–1568

Michele SD, Tassa A, Mugnai A, Marzano FS, Bauer P, Baptista JPVP (2005) Bayesian algorithm for microwave-based precipitation retrieval: Description and application to tmi measurements over ocean. Geoscience and Remote Sensing, IEEE Transactions on 43(4):778–791

Mlawer EJ, Taubman SJ, Brown PD, Iacono MJ, Clough SA (1997) Radiative transfer for inhomogeneous atmospheres: Rrtm, a validated correlated-k model for the longwave. Journal of Geophysical Research: Atmospheres (1984–2012) 102(D14):16,663–16,682

Mugnai A, Smith EA (1988) Radiative transfer to space through a precipitating cloud at multiple microwave frequencies. part i: Model description. Journal of Applied Meteorology 27(9):1055–1073

Mugnai A, Cooper HJ, Smith EA, Tripoli GJ (1990) Simulation of microwave brightness temperatures of an evolving hailstorm at ssm/i frequencies. Bulletin of the American Meteorological Society 71(1):2–13

Mülmenstädt J, Sourdeval O, Delanoë J, Quaas J (2015) Frequency of occurrence of rain from liquid-, mixed-, and ice-phase clouds derived from a-train satellite retrievals. Geophysical Research Letters 42(15):6502–6509

Noh Y, Cheon WG, Hong SY, Raasch S (2003) Improvement of the k-profile model for the planetary boundary layer based on large eddy simulation data. Boundary Layer Meteorology 107(2):401–427, DOI 10.1023/A:1022146015946

Omrani H, Drobinski P, Dubos T (2013) Optimal nudging strategies in regional climate modelling: investigation in a big-brother experiment over the european and mediterranean regions. Climate dynamics 41(9-10):2451–2470

Omrani H, Drobinski P, Dubos T (2015) Using nudging to improve global-regional dynamic consistency in limited-area climate modeling: What should we nudge? Climate Dynamics 44(5-6):1627–1644

Panegrossi G, Dietrich S, Marzano FS, Mugnai A, Smith EA, Xiang X, Tripoli GJ, Wang PK, Poiares Baptista JPV (1998) Use of cloud model

microphysics for passive microwave-based precipitation retrieval: Significance of consistency between model and measurement manifolds. Journal of the Atmospheric Sciences 55:1644–1673

Pastor F, Gmez I, Estrela MJ (2010) Numerical study of the October 2007 flash flood in the Valencia region (Eastern Spain): the role of orography. Natural Hazards and Earth System Sciences 10(6):1331–1345, DOI 10.5194/nhess-10-1331-2010

Pastor F, Valiente JA, Estrela MJ (2015) Sea surface temperature and torrential rains in the Valencia region: modelling the role of recharge areas. Natural Hazards and Earth System Sciences Discussions 3(2):1357–1396, DOI 10.5194/nhessd-3-1357-2015

Petty GW (1995) The status of satellite-based rainfall estimation over land. Remote Sensing of Environment 51(1):125–137

Piriou JM, Redelsperger JL, Geleyn JF, Lafore JP, Guichard F (2007) An approach for convective parameterization with memory: Separating microphysics and transport in grid-scale equations. Journal of the Atmospheric Sciences 64(11):4127–4139

Prein AF, Langhans W, Fosser G, Ferrone A, Ban N, Goergen K, Keller M, Tlle M, Gutjahr O, Feser F, Brisson E, Kollet S, Schmidli J, van Lipzig NPM, Leung R (2015) A review on regional convection-permitting climate modeling: demonstrations, prospects, and challenges: Convection-permitting climate modeling. Reviews of Geophysics DOI 10.1002/2014RG000475

Protat A, Pelon J, Grand N, Delville P, Laborie P, Vinson JP, Bouniol D, Bruneau D, Chepfer H, Delanoë J, et al (2004) Le projet rali: Combinaison d'un radar et d'un lidar pour l'étude des nuages faiblement précipitants. La Météorologie 47, DOI 10.4267/2042/36076

Protat A, Bouniol D, Delanoë J, May PT, Plana-Fattori A, Hasson A, O'Connor E, Görsdorf U, Heymsfield AJ (2009) Assessment of Cloudsat Reflectivity Measurements and Ice Cloud Properties Using Ground-Based and Airborne Cloud Radar Observations. Journal of Atmospheric and Oceanic Technology 26:1717, DOI 10.1175/2009JTECHA1246.1

Quintana-Seguí P, Le Moigne P, Durand Y, Martin E, Habets F, Baillon M, Canellas C, Franchisteguy L, Morel S (2008) Analysis of near-surface atmospheric variables: Validation of the SAFRAN analysis over France. Journal of Applied Meteorology 47(1):92–107, DOI 10.1175/2007JAMC1636.1

Ricard D, Ducrocq V, Auger L (2012) A climatology of the mesoscale environment associated with heavily precipitating events over a northwestern Mediterranean area. J Appl Meteor Climatol 51(3):468–488, DOI 10.1175/JAMC-D-11-017.1

Ruti P, Somot S, Giorgi F, Dubois C, Flaounas E, Obermann A, Dell'Aquila A, Pisacane G, Harzallah A, Lombardi E, Ahrens B, Akhtar N, Alias A, Arsouze T, Raznar R, Bastin S, Bartholy J, Béranger K, Beuvier J, Bouffies-Cloche S, Brauch J, Cabos W, Calmanti S, Calvet JC, Carillo A, Conte D, Coppola E, Djurdjevic V, Drobinski P, Elizalde A, Gaertner M, Galan P, Gallardo C, Gualdi S, Goncalves M, Jorba O, Jorda G, Lheveder B, Lebeaupin-Brossier C, Li L, Liguori G, Lionello P, Macias-Moy D, Onol B, Rajkovic B, Ramage K, Sevault F, Sannino G, Struglia MV, Sanna A, Torma C, Vervatis V (2015) Med-cordex initiative for mediterranean climate studies. Bull Am Meteorol Soc DOI 10.1175/BAMS-D-14-00176.1

Rysman JF, Claud C, Chaboureau JP, Delanoë J, Funatsu BM (2015) Severe convection in the mediterranean from microwave observations and a convection-permitting model. Quarterly Journal of the Royal Meteorological Society pp n/a–n/a, DOI 10.1002/qj.2611

Rysman JF, Lemaître Y, Moreau E (2016) Spatial and temporal variability of rainfall in the alps-mediterranean euroregion. Journal of Applied Meteorology and Climatology n/a:n/a–n/a, DOI 10.1175/JAMC-D-15-0095.1

Salameh T, Drobinski P, Dubos T (2010) The effect of indiscriminate nudging time on large and small scales in regional climate modelling: application to the mediterranean basin. Quarterly Journal of the Royal Meteorological Society 136(646):170–182

Sanò P, Casella D, Mugnai A, Schiavon G, Smith E, Tripoli GJ, et al (2013) Transitioning from crd to cdrd in bayesian retrieval of rainfall from satellite passive microwave measurements: Part 1. algorithm description and testing. Geoscience and Remote Sensing, IEEE Transactions on 51(7):4119–4143

Sanò P, Panegrossi G, Casella D, Di Paola F, Milani L, Mugnai A, Petracca M, Dietrich S (2015) The passive microwave neural network precipitation retrieval (pnpr) algorithm for amsu/mhs

observations: description and application to european case studies. Atmospheric Measurement Techniques 8(2):837–857

Saunders R, Matricardi M, Brunel P (1999) An improved fast radiative transfer model for assimilation of satellite radiance observations. Quarterly Journal of the Royal Meteorological Society 125(556):1407–1425

Saunders R, Matricardi M, Brunel P, English S, P B, Rayer P (2005) Rttov-8 science and validation report. NWP SAF Report 41

Saunders R, Hocking J, Rundle D, Rayer P, Matricardi M, Geer A, Lupu C, Brunel P, Vidot J (2013) Rttov-11 science and validation report. Tech. rep., Met Office, ECMWF, KNMI and Météo France

Simmons A, Uppala S, Dee D, Kobayashi S (2007) Era-interim: New ecmwf reanalysis products from 1989 onwards. ECMWF newsletter 110(110):25–35

Skamarock WC, Klemp JB, Dudhia J, Gill DO, Barker DM, Duda M, Huang XY, Wang W, Powers JG (2008) A description of the advanced research WRF version 3. Tech. rep., DTIC Document

Skofronick-Jackson GM, Gasiewski AJ, Wang JR (2002) Influence of microphysical cloud parameterizations on microwave brightness temperatures. IEEE Transactions on Geoscience and Remote Sensing 40:187–196, DOI 10.1109/36.981360

Smirnova TG, Brown JM, Benjamin SG (1997) Performance of different soil model configurations in simulating ground surface temperature and surface fluxes. Monthly Weather Review 125(8):1870–1884

Smirnova TG, Brown JM, Benjamin SG, Kim D (2000) Parameterization of cold-season processes in the maps land-surface scheme. Journal of Geophysical Research: Atmospheres (1984–2012) 105(D3):4077–4086

Smith EA, Cooper HJ, Xiang X, Mugnai A, Tripoli GJ (1992) Foundations for statistical-physical precipitation retrieval from passive microwave satellite measurements. part i: Brightness-temperature properties of a time-dependent cloud-radiation model. Journal of Applied Meteorology 31(6):506–531

Sodemann H, Zubler E (2010) Seasonal and interannual variability of the moisture sources for alpine precipitation during 1995–2002. International Journal of Climatology 30(7):947–961

Staelin D, Barrett A, Rosenkranz P, Barath F, Johnson E, Waters J, Wouters A, Lenoir W (1975) The scanning microwave spectrometer (scams) experiment. The Nimbus-6 Users Guide pp 59–86

Stéfanon M, Drobinski P, DAndrea F, Lebeaupin-Brossier C, Bastin S (2014) Soil moisture-temperature feedbacks at meso-scale during summer heat waves over western europe. Climate dynamics 42(5-6):1309–1324

Stephens GL, Kummerow CD (2007) The remote sensing of clouds and precipitation from space: A review. Journal of the Atmospheric Sciences 64(11):3742–3765

Surussavadee C, Staelin DH (2006) Comparison of amsu millimeter-wave satellite observations, mm5/tbscat predicted radiances, and electromagnetic models for hydrometeors. Geoscience and Remote Sensing, IEEE Transactions on 44(10):2667–2678

Surussavadee C, Staelin DH (2008a) Global millimeter-wave precipitation retrievals trained with a cloud-resolving numerical weather prediction model, part i: Retrieval design. Geoscience and Remote Sensing, IEEE Transactions on 46(1):99–108

Surussavadee C, Staelin DH (2008b) Global millimeter-wave precipitation retrievals trained with a cloud-resolving numerical weather-prediction model, part ii: Performance evaluation. Geoscience and Remote Sensing, IEEE Transactions on 46(1):109–118

Susskind J, Rosenfield J, Reuter D, Chahine M (1984) Remote sensing of weather and climate parameters from hirs2/msu on tiros-n. Journal of Geophysical Research: Atmospheres (1984–2012) 89(D3):4677–4697

Taylor KE (2001) Summarizing multiple aspects of model performance in a single diagram. Journal of Geophysical Research: Atmospheres 106(D7):7183–7192, DOI 10.1029/2000JD900719

Vangasse P, Charlton J, Jarrett M (1996) Characterisation of the advanced microwave sounding unit, AMSU-B. Advances in Space Research 17:75–78, DOI 10.1016/0273-1177(95)00451-J

Wang J, Wilheit T, Chang L (1989) Retrieval of total precipitable water using radiometric measurements near 92 and 183 ghz. Journal of Applied Meteorology 28(2):146–154

Weng F, Zhao L, Ferraro RR, Poe G, Li X, Grody NC (2003) Advanced microwave sounding unit cloud and precipitation algorithms. Radio Sci-

ence 38:8068, DOI 10.1029/2002RS002679

Wiedner M, Prigent C, Pardo JR, Nuissier O, Chaboureau JP, Pinty JP, Mascart P (2004) Modeling of passive microwave responses in convective situations using outputs from mesoscale models: comparison with TRMM/TMI satellite observations. Journal of Geophysical Research 109:D06214, DOI 10.1029/2003JD004280

Wu L, Li JLF, Pi CJ, Yu JY, Chen JP (2015) An observationally based evaluation of wrf seasonal simulations over the central and eastern pacific. Journal of Geophysical Research: Atmospheres pp n/a–n/a, DOI 10.1002/2015JD023561, 2015JD023561